Proceedings of the ASME 2013 32nd International Conference on Ocean, Offshore and Arctic Engineering
OMAE 2013
June 9-14, 2013, Nantes, France

OMAE 2013-10876

3D EFFICIENCY ANALYSIS OF CYCLOIDAL WAVE ENERGY CONVERTERS IN OBLIQUE WAVE FIELDS

Casey Fagley*

Atargis Energy Corporation
3185 Janitell Road Ste. 101
Colorado Springs, Colorado, 80906,
USA
Email: casey.fagley@atargis.com

Stefan G. Siegel

Atargis Energy Corporation
3185 Janitell Road Ste. 101
Colorado Springs, Colorado, 80906,
USA
Email: stefan@siegels.us

Jürgen Seidel

Atargis Energy Corporation
3185 Janitell Road Ste. 101
Colorado Springs, Colorado, 80906,
USA
Email: jurgen.seidel@atargis.com

Christian Schmittner

MARIN
2, Haagsteeg, P.O. Box 28
6700 AA Wageningen
The Netherlands
Email: c.schmittner@marin.nl

ABSTRACT

Numerical results from a 3D diffraction model are presented where a Cycloidal Wave Energy Converter (CycWEC) is interacting with an incoming straight crested Airy Wave. The diffraction model was developed in response to experimental observations from 1:10 scale experiments which were conducted in the Texas A&M Offshore Technology Research center wave basin. These experiments were the first investigations involving a CycWEC where three dimensional wave diffraction effects were present due to the fact that the span of the CycWEC was much smaller than the width of the basin. The diffraction model predicted the observed surface wave patterns in the experiment well, and showed that diffraction induced wave focusing increased the recoverable wave power beyond the 2D predictions for small CycWEC spans, while approaching the 2D limit for very large spans. The numerical model was subsequently used to estimate the sensitivity of the CycWEC to misalignment between the incoming waves and the WEC shaft. The loss in efficiency was found to be strongly dependent on the ratio between WEC span and incoming wavelength, where short spans (on the order of one wave length or less) which are realistic for actual ocean deployment showed only minor reductions in efficiency, while very long spans were found to be more sensitive to misalignment.

1 Introduction

Among alternative energy sources, wave power is one of the most abundant sources on earth. The World Energy Council according to [1] has estimated the world wide annual amount of wave power energy at 17.5 PWh (Peta Watt hours = $10^{12} kWh$). This amount of power is actually comparable to the annual world wide electric energy consumption, which is currently estimated at 16 PWh. Thus, wave power has the potential to provide a large portion of the worlds electric energy needs, if it can be harnessed

*Address all correspondence to this author.

efficiently. In addition to the energy availability, wave power has other advantages. Since a large portion of the worlds population lives close to the ocean shores, the distance between energy production and consumption is small, which reduces transmission losses and necessary investments in transmission lines. As opposed to other alternative energy sources like wind, stream and solar energy, the installation of wave power devices does not require use of already precious real estate. This makes wave power an ideal energy source for efficiently providing renewable energy to densely populated coastal areas. Ocean waves have a tremendous potential to provide clean renewable energy. Further engineering aspects of wave power as an energy source are appealing as well. While the power density of both solar and wind in typical favorable sites is in the order of $1\,kWm^{-2}$ [2], wave power in a typical North Atlantic wave that was considered in a related paper [3] (wave height of $H = 3.5m$ and period of $T = 9s$) yields $108\,kWm^{-1}$ of wave crest. As shown there, a device extending about $40m$ in the vertical direction can extract almost all of this wave power, yielding a power density of about $2.7kWm^{-2}$ or more than two and a half times that of wind or solar power. If one considers the theoretical inviscid conversion limits for waves and wind, which are 100% for waves [4] and 59% for wind [5], the accessible power density of waves is more than four times as large as that of wind. Furthermore, wave energy is available on a more consistent basis and can be better predicted in advance, therefore mitigating the need to back up a wave power plant with other conventional power sources, such as solar and wind energy.

2 Motivation and Objectives

Analysis of the different wave energy conversion devices that have been investigated or proposed reveals a number of commonalities in design. The first is that all devices require a connection to the sea bed in order to extract energy, which has two main drawbacks. First, a seabed connection makes the device vulnerable in rough seas and storms, in the same way as an anchored ship is vulnerable in a storm (and will likely break the anchor line). According to [1], storm survivability has been a major problem for many wave energy converters, with some being destroyed by the elements as early as during deployment. Also, for most of the devices, the load imposed onto the seabed connection is proportional to the power which the device can extract. This means that the anchor point needs to be stronger and thus more costly as more energy is being extracted. Therefore, many of these devices cannot easily be scaled up to industrial power plant levels of energy conversion. In addition, since the devices need to be anchored to the sea floor, they are not well suited to operation in deep water waves, where the ocean floor may be hundreds of meters away from the surface. However, most wave energy is contained in deep water waves, and the energy density of a wave decreases as it approaches shallow water. Thus, most devices cannot operate in the most promising locations for wave power extraction.

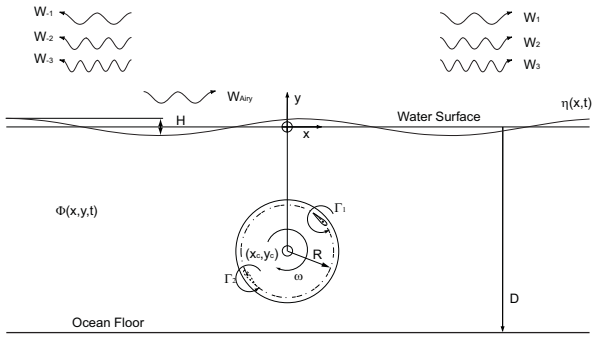

Figure 1. Cycloidal wave energy converter geometry and generated waves

Beyond survivability, efficiency has been a major issue for many WEC designs. While wave energy as a resource may be free, the construction effort to harness it is a major expense and to a large degree determines the cost of energy being produced. As a less efficient WEC will need to be larger in size to extract the same amount of energy as a more efficient one, cost of energy is directly related to efficiency. Arguably, the most efficient WEC is one that can extract all of the energy from an incoming wave, and the class of wave energy converters that is able to achieve this is commonly referred to in literature as wave termination devices. There have been various wave termination designs reported in literature, with the most well known devices being the Salter Duck [6] and the Bristol or Evans Cylinder [7]. Both consist of a series of elements which are aligned parallel to the wave crests, in the case of the Salter Duck these are cam–shaped and floating on the surface, while the Bristol Cylinder is fully submerged. Both have been shown to be able to absorb an incoming wave completely. The wave energy is converted to electric power by means of a power–take–off system that is hydraulic in both cases. As both devices move at approximately the wave induced water velocity, the devices need to feature a large surface area to convert appreciable amounts of power. This increases construction cost, reduces storm survival odds and has ultimately motivated the investigation of the Cycloidal WEC described here. The fact that both devices require mooring to the ocean floor also hampers storm survival odds and precludes installation in very deep water.

A typical cycloidal wave energy converter (CycWEC) as considered in this paper is shown in figure 1. It features one or more hydrofoils attached eccentrically to a main shaft at a radius *R*. While the shaft rotates, the pitch angle of the blades may be adjusted. This device operates at a rotational speed of the hydrofoil that is typically an order of magnitude larger than the wave induced water velocity, and employs the lift force at the hydrofoil to generate shaft torque directly. Using lift allows for a much smaller hydrofoil plan form area to be employed com-

pared to the cross sectional areas of Duck and Cylinder, and generating shaft torque directly eliminates the need for a costly and inefficient hydraulic power take off system. In addition, it is conceptually possible to join several CycWECs into a cluster where the reactive forces at the shaft can be made to cancel, which reduces or negates entirely the need for mooring and thus enables deep water deployment while improving storm survival odds (see Siegel [8] for sketches). The fact that the reactive force changes direction though 360° with each wave passage enables force cancellation if the individual WECs are spaced half a wavelength apart, thus causing reactive forces of same magnitude but opposite direction.

A single rotating hydrofoil was first investigated by Hermans et al. [9] both numerically and experimentally. While Hermans et al. reported very low wave energy conversion efficiencies (on the order of a few percent), Siegel et al. [10] were able to show in simulations that with improved sizing of the WEC as well as by using synchronization of the rotation of the foil with the incoming wave, wave termination with better than 99% inviscid efficiency was possible. These numerical findings were confirmed by 1:300 scale experiments in 2011, as reported by Siegel et al. [11] where invisicid conversion efficiencies of greater than 95% were achieved in the same facility employed in this study. Both of these initial studies performed synchronization of the WEC with a numerically generated harmonic wave, or a paddle wave maker, respectively. Thus they did not require a feedback controller and estimator to succeed. A controller and estimator were for the first time successfully implemented by Jeans et al. [12] for irregular waves in a numerical simulation. Typical conversion efficiencies in this study were beyond 90% for a superposition of two harmonic waves, and around 80% for irregular waves following a Bretschneider distribution. At the same time, the controller and estimator were successfully tested in an experiment as reported in [13] where harmonic waves with different wave heights and frequencies were successfully cancelled, achieving efficiencies comparable to the earlier synchronization experiments that had a priori knowledge of the incoming wave. The performance of the feedback controller and estimator could thus be experimentally verified for the first time. Next, the CycWEC investigations were advanced by experimentally canceling both a superposition of two harmonic waves, as well as irregular waves following a Bretschneider distribution. This has been done in simulations reported by Jeans et al. [12], as well as experimentally validated by Siegel et al. [14] in a small 2D wave flume .

The first wave cancellation experiments in a wave tank where the span of the WEC was far smaller than the width of the tunnel were conducted in 2012 at the Texas A&M Offshore Technology Research Center and established successful electricity production for the first time, see Fagley et al. [15]. Experimental observations also indicated the presence of 3D diffraction and wave focusing effects, and an initial version of a numerical model described in Fagley et al. [15] found good agreement between experiment and numerical model. In this work, we further refine this diffraction model and investigate the sensitivity of the CycWEC to angular offsets between WEC shaft and wave crest direction. This is of importance to predict possible efficiency reductions as a result of misalignment. It is also necessary to quantify the necessary accuracy of wave measurement equipment employed for alignment of WEC and incoming wave.

3 3D Wave Model

The surface elevation c of a circular wave can be described as, $\eta_c(x,z,t) = H(r)\sin(\omega t - kr)$ with X and Z the wave travel and wave normal coordinates, k the wave number, $r = \sqrt{(X-X_0)^2 + (Z-Z_0)^2}$ the distance from the wave center, T the wave period and t time. If this wave is to conserve energy as it radiates outward, the wave height H has to decrease with distance from the wave generator. If the initial wave height is specified as H_0 at a finite distance r_0 from the center,

$$H(r) = \sqrt{\frac{H_0^2 r_0}{4r}}, \tag{1}$$

the wave height does conserve wave energy resulting in a reduced wave height as the wave propagates away from the wave center at a $1/r$ relationship.

The initial version of the numerical diffraction model employed in this study has been reported in Fagley et al. [15]. There, the WEC generated wave was synthesized from a superposition of semi-circular waves according to equation 1. A typical semi-circular wave of this type is shown in figure 2 and features equal wave height for all azimuthal locations at a given distance from the source. Since the CycWEC produces single sided waves as reported in Siegel et al. [10], the left two quadrants are set to zero. This leads to an abrupt transition from zero to full wave height along the x=0 axis, and caused discrepancies between numerical model and experimental observations and wave gauge measurements. To improve this behavior, the present results use a modified circular point source,

$$\begin{aligned} H(r,\theta) &= \sqrt{\frac{H_0^2 r_0}{4r}}\cos\theta \\ \theta &= \arctan\left(\frac{Z-Z_0}{X-X_0}\right), \end{aligned} \tag{2}$$

where the wave height is modulated in the azimuthal direction as a function of the angle θ between wave travel direction and

spatial location at the surface. The resulting surface wave pattern is shown in figure 3 and features a maximum wave height in the positive wave travel direction, and zero wave heights in the positive and negative wave crest directions. The physical argument why this distribution is appropriate for modeling the WEC wave is related to the travel speed of the hydrofoil in the wave propagation direction: Along the X axis, the hydrofoil moves with the rotational speed in the direction of the wave propagation (the X axis). Conversely, along the Z Axis the hydrofoil travel velocity and the wave propagation direction (the Z axis) are perpendicular, thus creating no wave in that direction. For all angles in between, a cosine function describes the component of the hydrofoil velocity aligned with the wave propagation direction. Beyond this physical argument, it will be shown in the results chapter that this model provides better agreement with experimental data. It also avoids the abrupt wave height transitions of the semi-circular model.

It is possible to use several semi-circular waves to approximate the wave pattern caused by more complex wave generators. For a CycWEC, the waves generated can be approximated as a sum of individual semi-circular wave generators arranged along a line of finite length equal to the span S of the WEC blades, as shown by

$$\eta_{WEC}(x,z,t) = \sum_{n} \eta_{cn}, x > 0. \tag{3}$$

Single sided wave generation is assumed and assured by setting the WEC wave to zero for negative x coordinates, and is experimentally verified in following chapters. For a WEC perfectly aligned with the incoming wave, the N circular wave generators are located between $Z = -S/2$ and $Z = S/2$ along $X = 0$. A number of $N = 25$ individual circular waves was found to produce converged results. The strength of each circular wave generator used to discretize the WEC wave generation along the span of the hydrofoil was approximated by either a constant or an elliptical distribution according to the following equation:

$$H_0(z) = H_c\sqrt{(1-(\frac{z}{2S})^2}. \tag{4}$$

This modeled the lift distribution along the span of the foil which caused a wave height that was proportional to the local circulation which is shown in 2D potential flow simulations in Siegel et al. [10]. To assure that the maximum wave height at the center of the foil was H_c, the overall generated wave height was renormalized to the value specified. The wave field generated by the WEC was then superimposed with the wave field generated by the incoming wave. The incoming wave in this investigation

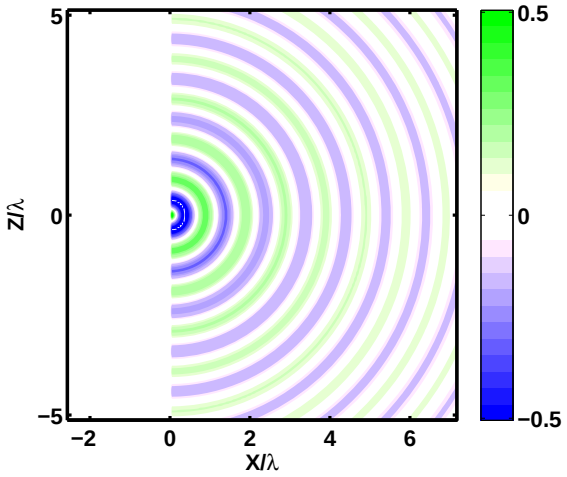

Figure 2. Surface Elevation of a fundamental circular wave with constant radial wave height

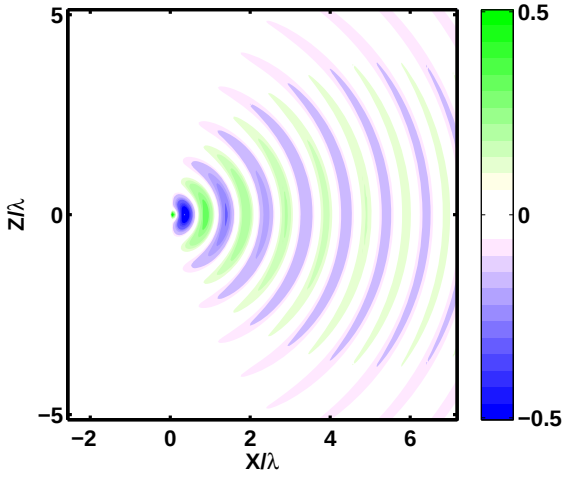

Figure 3. Surface Elevation of a fundamental circular wave with cosine modulated radial wave height

was a long crested Airy wave traveling in the positive X direction modeled as, $\eta_A(x,z,t) = H\sin(\omega t - kx)$ The final surface elevation was then calculated by superimposing the incoming airy wave with the wave generated by the WEC.

3.1 Control Volume analysis

The wave field resulting from the interaction of incoming Airy wave and the waves generated by the semi-circular waves used to model the WEC were used to determine the overall energy absorbed by the WEC. Using a control volume that enclosed the WEC completely, the fundamental waves entering and leav-

ing that control volume could be calculated. To ease calculations, the control volume chosen was a rectangle aligned with the coordinate system axes. The circular waves were decomposed in a X and Z component. Thus, the portion of each circular wave leaving the control volume boundaries could be calculated at each location along the boundaries. For an Airy wave, wave power P per unit length can be calculated as

$$P = \frac{\rho g}{8} H^2 C_g, \tag{5}$$

where C_g is the wave Celerity, ρ the density of water and g the gravity constant. Thus the wave power traversing a control volume boundary extending in the z direction from Z_1 to Z_2 could be calculated by

$$P = \int_{z_1}^{z_2} \sum_{m=1}^{M} P_{mx}(z) dz \tag{6}$$

$$P_x(z) = \frac{\rho g}{8} (H_x^2 + H_z^2) C_{gx}. \tag{7}$$

The subscripts indicate the vector component of the respective quantity in that direction. These equations can be modified to calculate the power traversing across a horizontal control volume boundary by swapping the subscripts X and Z. The overall amount of power extracted by the WEC could then be calculated by choosing a closed rectangular control volume and accounting for all wave power being transported across its boundaries. To determine the efficiency with which the WEC extracted energy from the waves, a reference quantity equal to the wave power of the Airy wave times the extend of the WEC in the Z direction was used. Thus, if the control volume analysis showed that this amount of energy was extracted from the waves, the efficiency was unity or 100%. Any efficiency larger than this indicated that diffraction induced wave focusing was encountered, while efficiencies below 100% indicated losses due to waves being radiated in the wave crest direction, or increases in wave height due to interaction between WEC wave and incoming wave as a result of ill matched phase. The control volume analysis was subjected to a convergence study in both control volume size, as well as discretization interval. These investigations yielded a control volume of equal extent in the wave travel (X) and wave crest (Z) directions of 20 wave lengths in size, as well as a minimum interval between control volume discretization of 1/10 of a wave length for convergence. Small residual periodic fluctuations in the resulting wave power were averaged over one period in space.

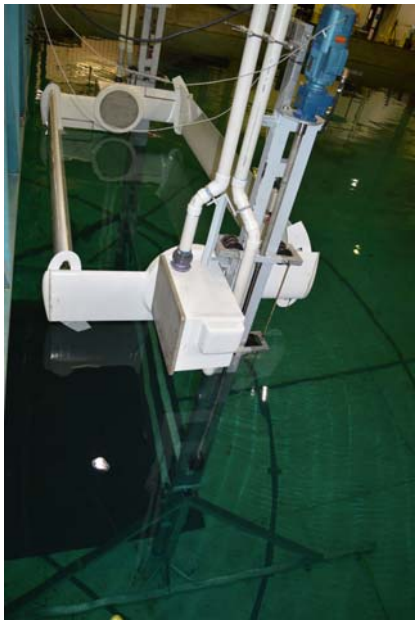

Figure 4. CycWEC 1:10 scale model installed in OTRC wave tunnel. The WEC is lifted above the water line during installation

4 Experimental Setup

4.1 Wave Basin

All experiments reported here were conducted at the Texas A&M University Offshore Technology Research Center (OTRC) wave basin. The basin was 45.7m in length, 30.5m in width and had a water depth of 5.8m. A set of 48 hinged flap wave makers, individually controlled by hydraulic cylinders, spanned one of the short sides of the basin. At the other end, a progressive wave absorber consisting of stacked screens acted as an artificial beach to reduce reflection of incoming waves. The wave maker had a maximum design wave height of $H_{WM} = 0.9m$ at a wave period of $T = 2.5s$. This wave was a deep water wave with a wave length of $\lambda = 9.75m$ and thus determined the model scale of 1:10 compared to a full scale deep ocean design wave for the CycWEC. While current and wind generators were available, they were not used in the present investigation. In order to investigate the surface wave pattern caused by the WEC and its interaction with incoming waves, a set of 10 wire type capacitive wave gauges were installed at a distance of 8m from the shaft of the WEC. The locations of the wave gauges are shown in figure 5. The wave gauge calibration was estimated to be accurate to within 1mm of water level. For all waves generated, a calibration was performed with the model removed from the water in order to assure that the wave heights at the model location matched the target values. For this calibration, a wave gauge was placed at the center of the model.

4.2 Cycloidal WEC Model

The CycWEC model, shown in figure 4, was designed specifically to efficiently interact with the wave climate in the OTRC tunnel. It featured two hydrofoils with a chord length $C = 0.75m$ and span $S = 4.5m$. The hydrofoils had a NACA0015 cross section with a curved camberline that matched the radius R=1m at which they were attached to the main shaft. End discs with a height of 10cm were installed at the ends to minimize tip vortex losses. The hydrofoils were attached to a split main shaft by means of two struts located at the ends of the hydrofoils. The struts were equipped with linear actuators allowing for control of the hydrofoil pitch. Each of the struts was streamlined with a NACA 0015 hydrofoil section. The main shafts were connected to two individual motor/generator units installed in water proof enclosures. These consisted of 3 Phase 230V AC 3.7kW asynchronous motors coupled to 80:1 gear boxes. The shafts were instrumented to allow for direct measurement of the shaft torque by means of two load cells. The load cells were calibrated by the manufacturer and delivered an accuracy of 0.05% of their full scale reading, which coincided with the maximum motor torque. The shaft angle was measured directly using incremental rotary encoders for position feedback. The motors were operated by four quadrant capable inverters allowing for software control of torque, speed and position. These inverters were also electronically linked to allow for synchronous rotation of both shafts. Breaking resistors allowed for dissipation of the regenerative power produced during wave power extraction. As the inverters were operated over a CANOpen network, pertinent parameters such as shaft position, velocity and motor current were reported back to the control computer and logged in sync with all other data. The motor current readings had a resolution of 0.1% of the nominal motor current. While the motors themselves were installed in water proof enclosures, the respective inverters were located in an electronics rack located on the bridge spanning the tunnel. This rack also accommodated the control computer used for feedback control of the WEC as well as for data acquisition and logging.

A mounting frame allowed for attachment of the WEC to hard points in the tunnel floor. While this provided a fixed horizontal positioning of the WEC in the tunnel, the WEC model itself could be traversed in the vertical direction by means of two lead screws operated by gear motors, which allowed access to the model when lifted above the water line and adjustment of submergence depth of the model during operation. The range of motion was $-1.8m < y_c < 1.2m$ and could be controlled with an accuracy of a fraction of a millimeter. Figure 4 shows the CycWEC model installed on the frame in the OTRC tunnel, while lifted out of the water.

All communication with motor controllers, pitch actuators and data acquisition was accomplished through a CAN bus network under a CANOpen software protocol. The feedback control software was run on a PC and written in LabVIEW, operating at an update rate of 20ms. All data logged during the experimental runs was synchronized using the CANOpen SYNC message ensuring that the measurements were taken at the same instants of time. The SYNC message also provided hardware based timing for the control loop providing feedback to the CycWEC.

5 Results

The following chapters outline results and observations from the experiment, followed by a comparison between the experimental data and the numerical result. The last two subsections in this chapter finally present numerical results for interaction of incoming wave and WEC shaft in alignment, followed by results where the WEC and incoming wave are skewed at varying angles.

5.1 Experimental Observations

Beyond shaft power and reactive force measurements reported elsewhere [15], the OTRC wave tunnel was equipped with 10 capacitive wave gauges for this experiment. These were arranged equidistant at a distance of 8m to the CycWEC, which was placed in the center of the wave basin as shown in figure 5. The CycWEC could be operated both in wave cancellation mode where energy was extracted from an incoming wave, or in wave generating mode where motor power was used to rotate the blades which subsequently created a single sided wave as reported in Fagley et al. [15]. The color contour overlay in figure 5 shows an incoming wave being canceled by the CycWEC, with the wave traveling in the positive X direction. A typical diffraction pattern due to the interaction between the WEC generated wave and the incoming wave can be seen to the right of the WEC, which is centered at X=0 and Z=0.

This WEC diffraction pattern could be observed in the wave tank experiment, figure 6 shows both the incoming and WEC waves impacting the screen system designed to prevent wave reflections. As the upper end of the screens provides a visual reference to visually gauge the water elevation at the screens, the modulated wave pattern across the tunnel can be well observed. This pattern indicates interaction of the WEC with the incoming waves, in the process of which wave energy is extracted. Without the WEC present or with the WEC at rest (not shown), the waves impacting the screens form a straight line of constant surface elevation across the wave basin, which fluctuates in height with the passage of each wave.

Thus the surface elevation observation shown in figure 6 provided qualitative evidence of wave energy extraction, while the next chapter compares qualitative data from both experiment and numerical simulation.

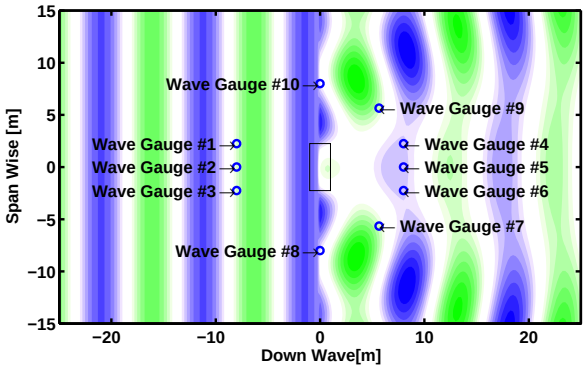

Figure 5. Instantaneous surface elevation for a wave generation simulation. WEC model is shown to scale as a rectangle, and the wave gauge locations are shown.

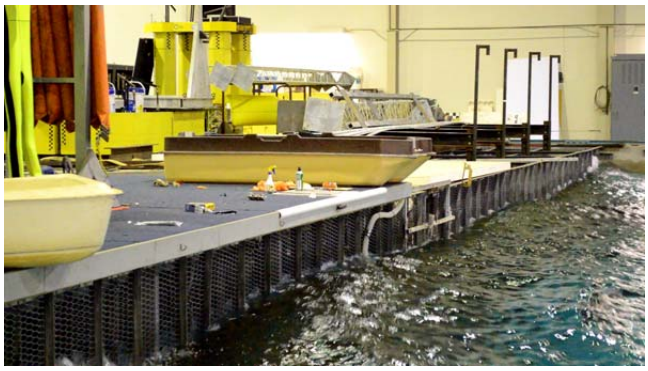

Figure 6. Picture of waves impacting screens at the end of the test section during an experimental wave cancellation run

5.2 Validation of Diffraction Model

In order to establish the validity of the numerical model beyond the first order rationale underlying its derivation as outlined in the numerical setup chapter, wave gauge data from the experiment was compared to predictions from the numerical model. Figure 7 shows data from a wave generation experiment where no incoming wave was present, in comparison to the numerical model predictions. It can be seen that all wave gauge measurements located down-wave from the WEC agree well with the numerical model. The numerical model data shown in figure 7 employed a cosine modulation of the point sources, which improved the match between numerical model and experimental data significantly compared to earlier results presented in Fagley et al. [15] where a constant azimuthal wave height was assumed. The improvement is most pronounced for wave gauges #7 and #9, which are located down-wave at an angle of 90 degrees from

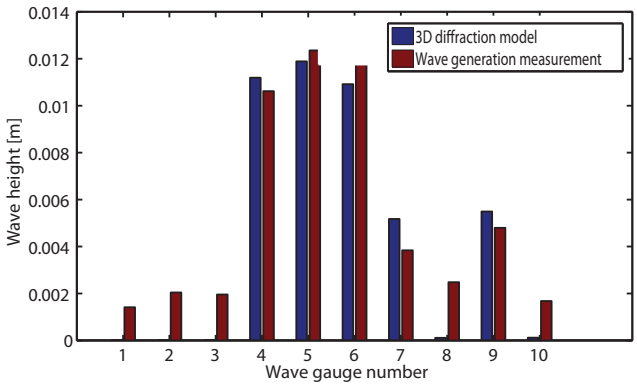

Figure 7. Comparison of wave heights from experimental measurements to predictions from the 3D diffraction model

the tip of the WEC blade. In all portions of the wave field that are dominated by the WEC–wave interaction (i.e. wave gauges #4 - #9), the agreement between numerical model and measurements can be seen to be very good.

The largest discrepancies between measurements and numerical model can be observed up-wave of the WEC, where wave reflections in the experiment led to larger wave heights than what was predicted by the numerical model which assumed these to be zero by design. The experimental measurements down–wave of the WEC showing the largest discrepancies were at wave gauge locations #8 and #10, where the measurements were again larger than the numerical estimates. These were similar in magnitude to those observed up–wave of the WEC, and thus most likely caused by reflections just as those up–wave of the WEC.

While one particular data set is shown, the agreement between experiment and numerical simulation was improved for all experimental data by employing cosine azimuthal modulated point sources. The data set shown in figure 7 is representative of all measurements taken. Further comparison between experiment and numerical model was made and reported in Fagley et al. [15], which is why the present comparison for brevity is limited to demonstration of the improvement due to the cosine modulation.

5.3 Diffraction Efficiency for aligned WEC and Waves

With a azimuthal modulation of wave height introduced to the numerical model, the initial investigation focused on development of an understanding of the impact of this modulation on wave energy conversion efficiency. Figure 8 compares the efficiency of two different radiation models (constant or top hat, and cosine modulated) along with two different span wise lift distribution models (again constant or top hat, and elliptical as described by equation 4). While the ratio between the incoming wave height and the wave height generated by the WEC at its

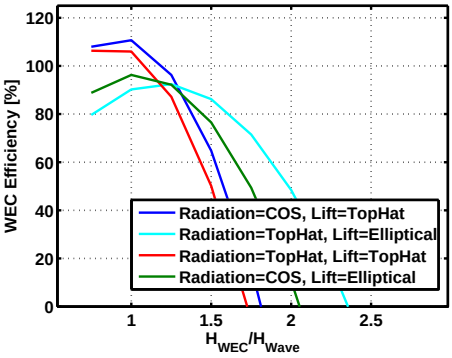

Figure 8. Wave Cancellation efficiency as a function of the ratio between incoming wave height and center height of the WEC generated wave. $Slambda = 2.\ T = 2.5s$

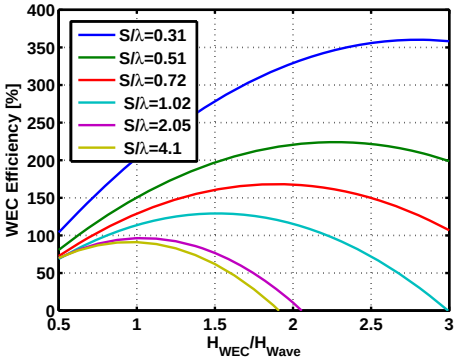

Figure 9. Wave cancellation efficiency and WEC Wave Height as a function of the ratio between incoming wave height and center height of the WEC generated wave for different Span to Wavelength Ratios. $T = 2.5s$

center was varied, all other parameters were kept constant.

It could be observed that the top hat lift distribution led to a higher maximum efficiency regardless of radiation pattern and at a relatively small height ratio. This could be attributed to the good match between the incoming (constant height along the crest) wave and the equally constant wave generated by the WEC. The two simulations using a elliptical lift distribution required a higher height ratio to achieve optimal wave cancellation efficiency, and did not achieve the same efficiency but rather fell short by about 10 percent compared to the constant lift distribution. The higher height ratio correlated well with the smaller average wave height produced by an elliptical lift distribution, which was reduced by a factor of $\pi/4$. From the data in figure 8 it could be concluded that a more realistic lift distribution (where an elliptical lift distribution constitutes an optimal situation in terms of hydrofoil induced drag) carried a penalty of about 10% in efficiency, compared to top hat distribution that was only achievable in a theoretical study like the present one but could be seen to be favorable in terms of diffraction efficiency. The impact of the radiation distribution on efficiency was less prominent, and at peak efficiency only caused a difference of a few percent. The cosine radiation distribution however could be seen to be favorable by a small margin for both lift distributions.

The data presented in all following figures was obtained using the cosine radiation distribution along with the elliptical lift distribution. In order to determine the optimal wave height ratio for a range of different span to wavelength ratios, a parameter study was conducted. Figure 9 shows that there existed an optimal height ratio for each WEC span. This height ratio was larger for smaller spans, and also resulted in an overall larger efficiency. For small WEC spans, efficiencies in excess of 350% could be observed, indicating strong diffraction and wave focusing effects. These results were in excess of our earlier findings using a constant radiation distribution. This was due to the fact that less

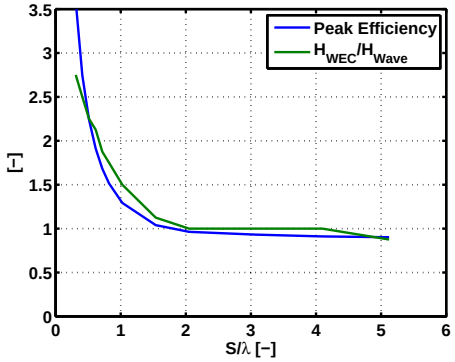

Figure 10. Optimum wave cancellation efficiency and WEC Wave Height as a function of the ratio between WEC Span and wavelength. $T = 2.5s$

wave power was lost in the span wise direction in the present cosine modulated numerical model, compared to the original constant radiation model. For very large WEC spans, however, the peak diffraction efficiency dropped below 100% as a result of the increased non-uniform span wise lift distribution.

For control design purposes, the relationship between WEC Wave height and WEC span for optimum power extraction was of interest. Figure 10 shows this relationship along with the resulting optimal efficiency.Both required wave height and efficiency were almost identical and reflected the underlying conservation of power of the numerical model.

In summary, the results of the cosine modulated radiation distribution surpassed those presented earlier for a constant azimuthal radiation model. A constant lift distribution however would (if it were achievable) perform better than a more realistic elliptical lift distribution.

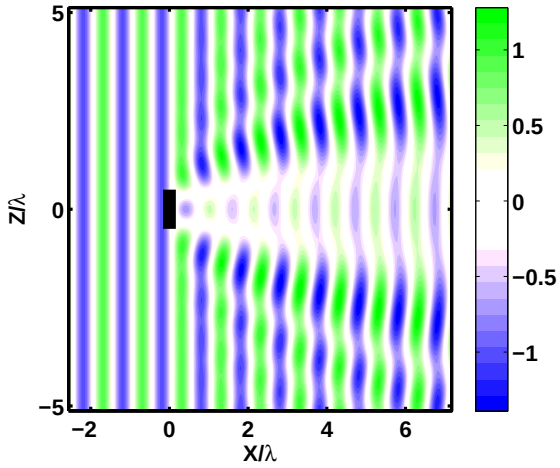

Figure 11. Surface Elevation during wave cancellation with a WEC of size $S/\lambda = 1$ at angle $\alpha = 0^\circ$ to the waves

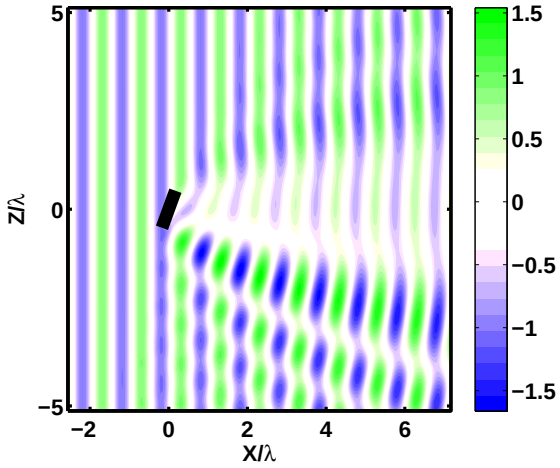

Figure 12. Surface Elevation during wave cancellation with a WEC of size $S/\lambda = 1$ at angle $\alpha = 20^\circ$ to the waves

5.4 Diffraction Efficiency for WEC and Waves at an angle

The interaction between a CycWEC and an incoming straight crested wave always led to a symmetric radiation pattern, if the WEC shaft was aligned with the wave crests. A typical surface wave pattern is shown in figure 11 for a span equal to one wavelength. The angle of the first maximum of the wave crests relative to the wave travel direction was a direct function of the span to wavelength ratio, as was shown in Fagley et al. [15]. While perfect alignment is obviously the optimal configuration for this type of wave energy converter, this chapter explores the impact that misalignment has on WEC performance, as well as on the wave radiation pattern.

With all other parameters kept the same, the surface radiation wave patterns shown in figure 12 and figure 13 show the effects of an angle of 20° and 45° between WEC shaft and incoming wave crests, respectively. The WEC was rotated about its center for these investigations, which led to a positive phase error at one tip of the WEC, and an equal magnitude but opposite sign phase error at the other tip due to the displacement of the tip relative to the Z axis. The resulting diffraction pattern show undisturbed waves in the upper portion of the wave field, and short crested waves in the lower portion. In both cases the wake in the wave pattern was not as pronounced as in the aligned situation shown in figure 11.

A parameter study where both WEC span as well as the angle between the incoming wave and the WEC shaft were varied was conducted next. Figure 14 shows that there is a dramatic impact of the WEC span on the resulting efficiency loss for a given angle, with larger spans causing a larger reduction in efficiency.

A study was conducted varying the wave height ratio between incoming wave and wave generated by the WEC for all

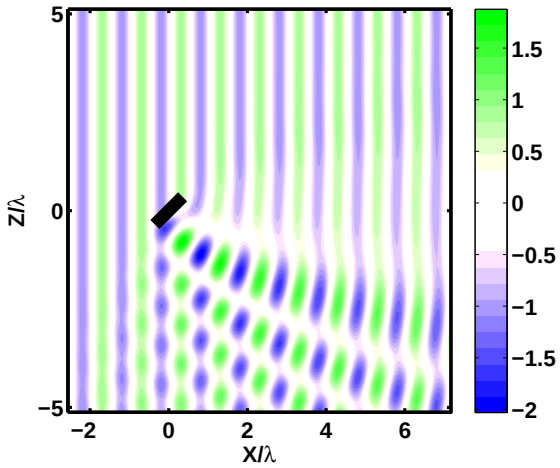

Figure 13. Surface Elevation during wave cancellation with a WEC of size $S/\lambda = 1$ at angle $\alpha = 45^\circ$ to the waves

angles shown in 14. While not shown, varying the height ratio did not improve the efficiency. Similarly, the feedback phase between the incoming wave and the WEC wave was varied in a second study to investigate if a different phase than what was optimal for zero angle would be advantageous. This study also found no improvement in efficiency for variations in feedback phase. As the phase at the center of the WEC was identical for all angles to that of the zero angle situation, and the left end of the WEC had a phase lag equal in magnitude and opposite in sign to the right end of the WEC, this behavior was to be expected since the average phase mismatch would only increase for different feedback phases.

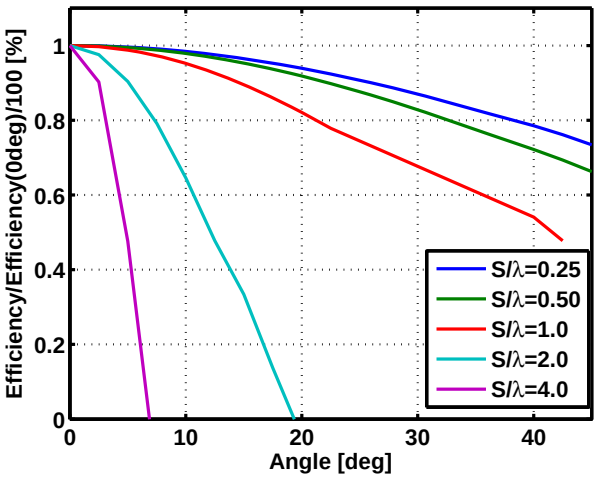

Figure 14. Wave Cancellation efficiency as a function of angle between WEC and Wave Crest for different WEC spans

6 Conclusions

In order to understand and isolate the impact of diffraction on the CycWEC performance, a simple 3D diffraction model was developed based on linear circular point wave source superposition. Two different types of point sources were investigated, and the point source with a cosine modulation of the wave height was found to provide better agreement compared to a constant wave height for all angles. The model agreed well with measured wave heights measured in a 1:10 scale experiment experiment, and showed that wave diffraction induced wave focusing increased the wave power that could be extracted beyond the two dimensional limit. This indicated that while the CycWEC avoided the losses due to up-wave radiated waves suffered by typical symmetric point absorbers, it could nonetheless leverage the benefits of diffraction induced wave focusing at small span to wave length ratios.

The numerical model was then used to investigate the sensitivity of the CycWEC to angular misalignment between WEC shaft and incoming wave crests. The sensitivity was found to be strongly dependent on the ratio between span of the WEC and incoming wavelength. For short spans the reduction in power extraction efficiency was minor, while very large spans showed a drastic reduction in efficiency. This loss in efficiency could be attributed to a mismatch in phase between the incoming wave and the WEC, which increased with increasing span due to the larger displacement of the WEC blade tips relative to the incoming wave front.

REFERENCES

[1] Boyle, G., 2004. *Renewable Energy - Power for a sustainable future*. Oxford University Press.

[2] Bedart, R., 2005. Final summary report - offshore wave power feasibility demonstration project. Tech. rep., E2I EPRI Global, WP 009 - US Rev 1.

[3] Siegel, S. G., Fagley, C., and Nowlin, S., 2012. "Experimental wave termination in a 2d wave tunnel using a cycloidal wave energy converter". *Applied Ocean Research,* ***38***, October, pp. 92–99.

[4] Evans, D. V., 1976. "A theory for wave-power absorption by oscillating bodies". pp. 1–25.

[5] Betz, A., 1920. "Das maximum der theoretisch möglichen ausnützung des windes durch windmotoren". *Zeitschrift für das gesamte Turbinenwesen,* ***26***, p. 307309.

[6] Salter, S. H., 1989. "World progress in wave energy-1988". *International journal of ambient energy,* ***10***(1), pp. 3–24.

[7] Evans, D. V., Jeffrey, D. C., Salter, S. H., and Taylor, J. R. M., 1979. "Submerged cylinder wave energy device: theory and experiment". *Applied Ocean Research,* ***1***(1), pp. 3–12.

[8] Siegel, S. G., filed in 2006, awarded 2010. "Cyclical wave energy converter". *U. S. Patent 7,686,583 and pending / awarded International Patent applications*.

[9] Hermans, A. J., van Sabben, E., and Pinkster, J., 1990. "A device to extract energy from water waves". *Applied Ocean Research Computational Mechanics Publications,* ***Vol. 12, No. 4***, p. 5.

[10] Siegel, S. G., Jeans, T., and McLaughlin, T., April 2011. "Deep ocean wave energy conversion using a cycloidal turbine". *Applied Ocean Research,* ***Volume 33 Issue 2***, pp. 110–119.

[11] Siegel, S., Jeans, T., and McLaughlin, T., 2009. "Deep ocean wave cancellation using a cycloidal turbine". In 62nd Annual Meeting of the American Physical Society, Division of Fluid Dynamics, Minneapolis, MN.

[12] Jeans, T., Siegel, S. G., Fagley, C., and Seidel, J., 2011. "Irregular deep ocean wave energy conversion using a cycloidal wave energy converter". In 9th European Wave and Tidal Energy Conference (EWTEC),Southampton, UK, September 5th 9th.

[13] Siegel, S. G., Fagley, C., Roemer, M., and McLaughlin, T., 2011. "Experimental wave cancellation using a cycloidal wave energy converter". In 9th European Wave and Tidal Energy Conference (EWTEC),Southampton, UK, September 5th 9th.

[14] Siegel, S., Fagley, C., Roemer, M., and Mclaughlin, T., 2012. "Experimental investigation of irregular wave cancellation using a cycloidal wave energy converter". In 31st International Conference on Ocean, Offshore and Arctic Engineering (OMAE), no. OMAE2012-83388.

[15] Fagley, C., Siegel, S., and Seidel, J., 2012. "Wave cancellation experiments using a 1:10 scale cycloidal wave energy converter". In 1st Asian Wave and Tidal Energy Conference (AWTEC) Jeju Island, Korea, November 27-30.